EPRG-PRCI-APGA
23rd Joint Technical Meeting
Edinburgh, Scotland
6–10 June 2022

PAPER TITLE: CLOSED CONTROL LOOP FOR IMPRESSED CURRENT CATHODIC PROTECTION BASED ON CORROSION RATE SENSING
PAPER NUMBER: 18

Facundo (Bob) Varela*
Deakin University, School of Engineering, Victoria, Australia

Mike YJ Tan
Deakin University, School of Engineering, Victoria, Australia

* presenting author

ABSTRACT

Current CP systems use either static current output settings or a closed control loop based on potential measurements. Static output settings might lead to temporal and local over or under protection levels since they cannot adapt to changes in the environment. Closed control loops based on potential measurements have difficulties due to the IR-drop produced in typically resistive soils. This IR-drop can be large, limiting the information contained in potential measurements to only qualitative indications of the actual polarization achieved. Additionally, due to their construction, many types of standard reference electrodes often develop reliability issues when installed permanently in the field.

The recent development of electrode arrays has opened the possibility to close the control loop used for CP in a new and more reliable way. The external surface of electrode arrays can be made of epoxy and steel, therefore presenting a similar longevity to the assets they would sense. In addition, due to its electrochemical nature this method can be developed to provide almost instantaneous feedback of the status of the pipeline. Electrode arrays measure the distribution of current density over their surface and are therefore unaffected by IR-drops, allowing quantitative analysis of the collected data.

This project aims to perform a proof of concept on the development of a closed control loop for real-time adjustment of ICCP systems based on corrosion monitoring data from electrochemical probes. It was found that despite the non-linearities of the system induced by pH changes on the metal/soil interface a proportional controller was effective in compensating for system perturbations produced by IR-drops with high accuracy. The system performed well under static and dynamic initial conditions. Results from laboratory back-to-back tests comparing the new and traditional potential closed loops indicate that the new system provides a superior performance under stray current conditions.

DISCLAIMER

1. INTRODUCTION

Impressed current cathodic protection (ICCP) systems aim to polarize the structure they are applied to in the range of -850mV$_{CSE}$ to -1200mV$_{CSE}$ to be effective in preventing corrosion and avoid the negative effects of overprotection. In the early days of ICCP, systems such as the "Cumberland Electrolytic System"[1], the rectifiers used by Kuhn [2,3] and the first ICCP system in Australia [4], used variable resistors connected in series with the anodes as passive constant current supplies. This type of passive current supply is extremely inefficient due to the large conversion of electrical power into heat at the resistors and does not produce constant output. Most importantly, fixed current output is not suitable to compensate for the dynamic conditions experienced in many ICCP applications. Thus, several attempts for auto regulating systems were made before the invention and application of potentiostats for ICCP potential control [5,6,7]. At the heart of potentiostats there is an operational amplifier and the development of this electronic component is what made potentiostats possible [8,9]. Potentiostats are devices that continuously compare the potential difference between the working electrode (WE) and a reference half-cell (RE) against the desired set potential. If both potentials are not equal, the difference drives an amplifier that controls the amount of current flowing between WE and a counter electrode (CE). Potentiostats were first used in 1942 for academic research [10,11] (only one year after the invention of operational amplifiers) and by 1952 they were also being used for industrial applications such as electroplating [12].

Although the challenges regarding the electronics of ON-potential closed loop control for ICCP systems were overcome in the late 60's by solid state potentiostats [13,14,15,16], some additional complications related to the use of ON-potentials quickly became apparent. One of the issues was the unsuitability of reference half-cells to permanent field exposure, which can dry up and potentially lead to overprotection. The other mayor issue encountered was the significant IR-drop produced by the flow of the ICCP current in a non-zero resistance media. This IR-drop is unknown and dynamic, which makes difficult to evaluate the actual metal/environment interphase potential. By 1972, with the release of the NACE SP-0169 [17] and other standards [18,19], the effectiveness of CP was being defined in terms of IR-drop free potentials against the Cu/CuSO4 reference half-cell [17]. This triggered an era of developments that aimed to compensate or eliminate the IR-drops by performing instant OFF measurements [20,21,22,23,24]. Unfortunately, the current injected by ICCP systems is not the only source of IR-drop. Stray currents can also produce significant IR-drops, and these cannot be eliminated using the previous inventions. To mitigate this issue, IR-coupons were developed in the 1990's [25,26]. Although corrosion engineers have come a long way in characterising the effectiveness of CP in terms of electrode potential, it is important to keep in mind the limitations of this electrochemical parameter.

The metal/environment interphase potential is a purely thermodynamic parameter and therefore, contains no information regarding the kinetics of the corrosion process. If the objective of ICCP were to keep the structure within the immune region, the kinetics of the corrosion process would be of little importance, but this is not the case for most structures. For instance, for steel structures it is difficult to achieve immunity without significant generation of Hydrogen, which could result in coating damage and hydrogen embrittlement. Thus, the quest for a better way to identify the effectiveness of CP is not over.

Electrochemical corrosion monitoring methods could potentially be better suited to provide feedback for the control of ICCP systems since they evaluate corrosion rates directly. Stern and Geary presented one of the first electrochemical methods capable of measuring corrosion rates under cathodic polarization [27]. The main disadvantage of this method is that it requires assuming an idea behaviour for the cathodic curve (whether activation [27] or diffusion controlled [28,29]) which is extremely difficult to determine for the unknown and ever-changing conditions present in the field. In 1987, a more robust method was developed. This method is capable of evaluating corrosion rates over polarized metals by inducing a set of harmonic perturbations to a working electrode and obtaining electrochemical parameters such as Tafel coefficients for the currents recorded [30,31,32,33].

Unfortunately, this method requires precisely controlling the polarization of the sensing element during the measurement and this brings the same difficulties (IR-drop and unreliable reference half-cells) as those encountered to control ICCP systems through ON-potentials. An interesting alternative recently developed is the used of electrode arrays such as the Wire Beam Electrode [34]. Electrode arrays can be used to evaluate the distribution of current density on their surface without requiring knowledge of the potential at which is subjected. As discussed in previous publications [35,36,37,38,39,40], electrode arrays can be used to evaluate corrosion rates under CP with unprecedented sensitivity and also provide indications of overprotection.

2. EXPERIMETAL

2.1. Electrode array

A 100 element X65 steel electrode array in a 25 by 4 arrangement was used. Electrodes were squares of 2.24 mm in side spaces 0.3 mm apart. The 3D printed cover used to simulate a disbonded coating was designed to generate a 1mm crevice that covers 21 out of the 25 rows of electrodes. For all tests the electrode array was polished using 240 grit silicon carbide paper and running water as lubricant. Before the 3D printed cover was mounted onto the electrode array, a layer of the test soil was added over the electrodes. The intention behind this step is to ensure a continuous conductive path for the electrolyte within the crevice.

In order to measure the distribution of currents over the electrode array surface without interrupting CP, the instrumentation schematically illustrated in Fig. 1 was used. A multiplexer distributed the connections of the 100 electrodes in the array, maintaining 99 of them connected to the WE1 output terminal and the remaining electrode connected to the WE2 output terminal. In order to measure the current flowing throughout the electrode connected to WE2, a zero-resistance ammeter (ZRA) was interposed between WE1 and WE2. In addition to measuring currents, the ZRA kept WE1 and WE2 (i.e. all the electrodes in the array) at the same potential. The CP supplied to the array was managed by a Bio-logic VMP3 potentiostat in a three-electrode configuration, where WE1 acted as the working electrode. The current flowing throughout each electrode of the array was registered by swapping the electrode connected to WE2, following a predetermined sequence that swept the whole array. A make-before-break switching sequence between successive electrodes was followed to avoid any momentary disconnection of CP. Current distributions were measured consecutively, with a 10s pause in between measurements.

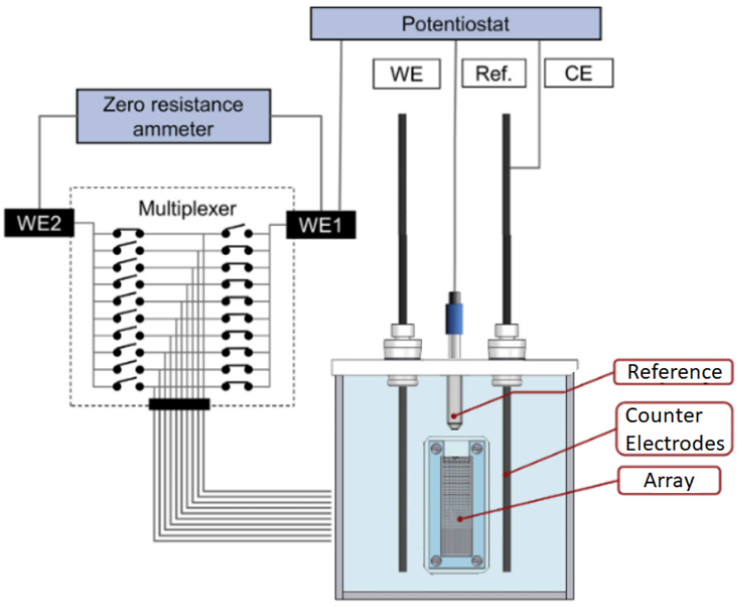

Figure 1, Schematic illustration of the instrumentation used.

2.2. Controller algorithm

The main objective of the control algorithm is to identify the output current required to achieve effective CP and avoid overprotection, while dynamically compensating for any perturbation that might be affecting the system. It uses the present current set point and the previous history of sensor readings as inputs to produce the next current set point as an output.

Figure 2 illustrates, in black, the core of the control algorithm. In a first stage the program reads the current applied to the structure by the ICCP system and the current density distribution on the surface of the electrode array. Then, the 100 current density values reported by the electrode array are processed into two critical values. One is the most anodic value and the other is the average current density for the electrodes located outside the crevice. If the most anodic value found is greater than zero, that current density value is considered the error and the algorithm increases the current output using a proportional controller (i.e. New current = Previous Current + Error. Kp, where Kp is the constant of the proportional controller). If, on the other hand, the most anodic current is zero, no corrosion is expected and then the decision is made on whether the system is protected or overprotected. At this stage, a fixed value of current density was used as a threshold to differentiate protection from overprotection.

This current density value represents the cathodic current density produced by the oxygen reduction reaction. The premise is that if the current density at the array surface is greater than that required to reduce all the oxygen that reaches its surface, the excess of current is used for the hydrogen evolution reaction which is directly associated with overprotection. Thus, if the average current density measured outside the crevice is greater than the threshold, this difference is used as the error and the algorithm increases the current output setting also using a proportional controller. (i.e. New current = Previous Current + Error. Kp).

For this study a controller of the proportional type was selected in favor of a more sophisticated proportional integrative derivative (PID) controller, due to its relative simplicity that simplifies troubleshooting and requires less tuning. PID controllers would reduce the settling time, but this potential benefit comes associated with several potential pitfalls such as integrator windup, susceptibility to noise and reduced bandwidth. In addition, the main factor currently limiting settling times is the high level of discretization produced by the slow refreshing time of the electrode array data (20 s). Thus, the potential benefits of a PID are small against the benefit produced by increasing the electrode array data acquisition rate.

In addition to the basic control algorithm, Figure 2 also includes in blue additional steps necessary to perform the test. At the beginning, the code generates a random current output setting that attempts to simulate the influence of stray currents and generates an Excel report sheet for the results. Then, populates the excel report and waits 20 s for the next measurement. From then on, the control algorithm is executed in a loop until no output current changes are required for 10 consecutive cycles. After that, a new random current fluctuation is generated and the compensation starts again until the test is manually stopped.

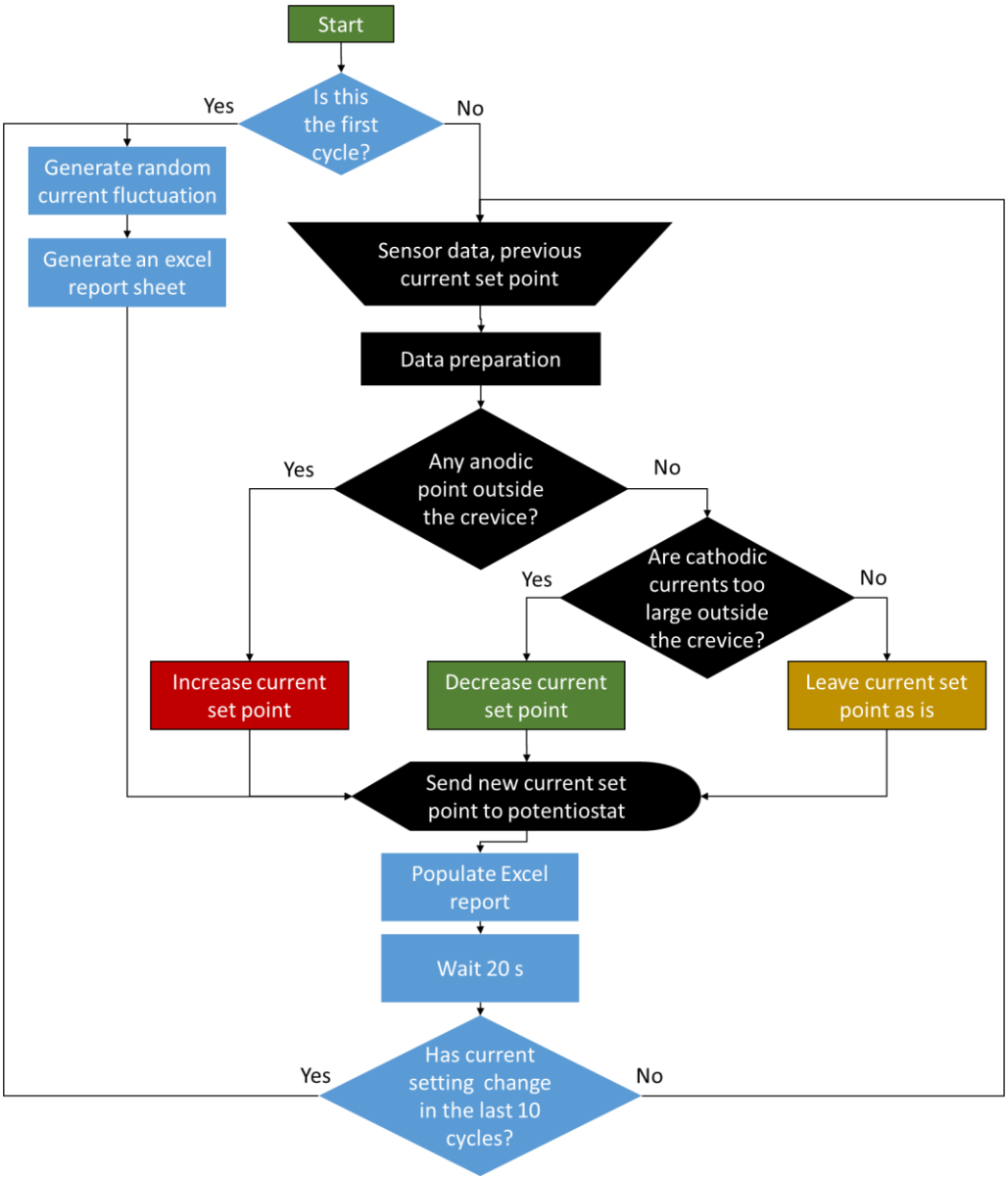

Figure 2. Controller algorithm flowchart.

2.3. Experimental arrangement for initial proof of concept

For the initial proof of concept, a 2.5L borosilicate electrochemical cell used. The cell has a flange connection at one side where the electrode array was installed. Fig. 1 illustrates this electrochemical cell with the electrode array installed. The two graphite counter electrodes were used as anodes and potentials were measured against a Luggin capillary where the Ag/Sat. AgC/Sat. KCl reference electrode was installed. The test environments used where mixes of sand and 0.01 M Na_2SO_4 at fractions of the sand water holding capacity (WHC). All tests were performed at 22±2ºC.

2.4. Experimental arrangement for back-to-back testing

The experimental arrangement used for these comparative tests is illustrated in Figure 3. The simulation of an infinite media is achieved by 50 outer Titanium electrodes (Outer electrodes in Fig. 3) that are maintained at the same electrical potential between them. When exposed to an uneven soil potential across the box, small currents flow among these electrodes, similarly to the current that would flow across the soil outside the box volume if this were a true infinite media. These small currents were constantly monitored throughout the tests (WBE data acquisition unit 2 in Fig. 3).

A reference electrode (REF 1 in Fig. 3) was placed at the end of the elongated part of the box. This is the remote electrode used as a remote reference for all potential measurements, even those controlling the CP unit when in autopotential mode. The remoteness of the reference electrode was confirmed by measuring vanishingly small currents on the Titanium outer electrodes and by constantly monitoring potential differences lower than 20 mV (potentiostat 3 in Fig. 3) between this reference electrode and another identical electrode (REF 2 in Fig. 3) located 20 cm away.

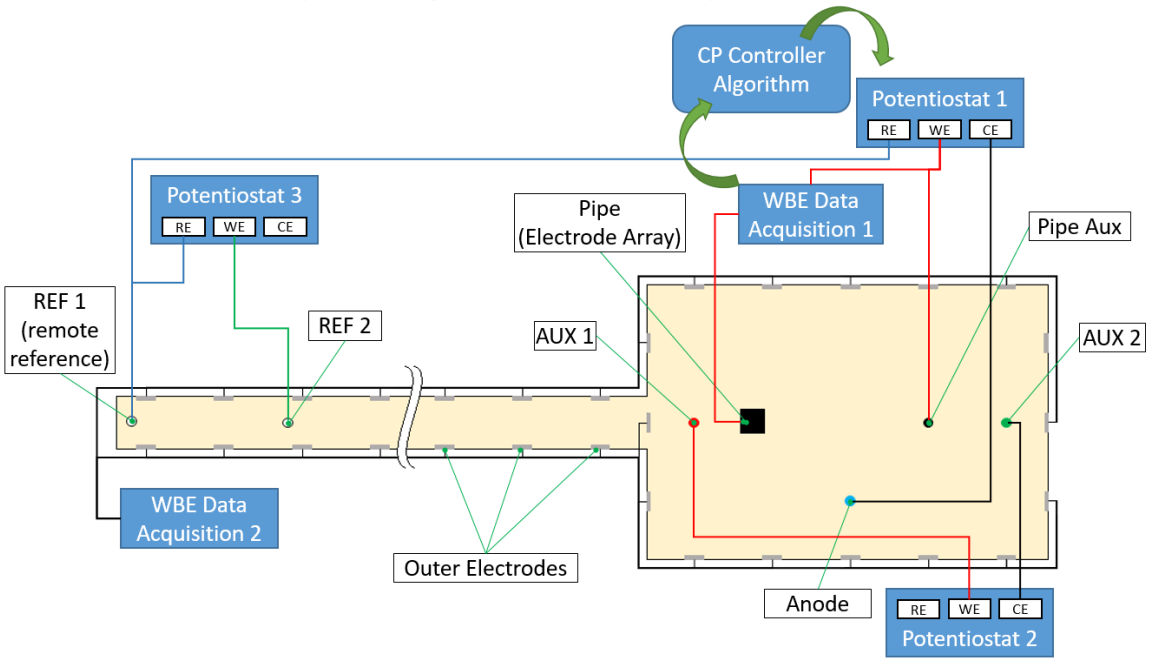

Figure 3. Experimental arrangement used for comparative test against autopotential control.

At the main section of the box, the pipeline was simulated using an electrode array (pipe electrode array in Fig. 3) and an auxiliary Ti electrode (pipe aux in Fig. 3). In order to induce stray currents on the simulated pipeline, a current was imposed (potentiostat 2 in Fig. 3) between two additional Ti electrodes (Aux 1 and 2 in Fig. 3). On this setup, a potentiostat (potentiostat 1 in Fig. 3) represents the CP rectifier and controls the current supplied to the anode (Anode in Fig. 3). When evaluating the conventional potentiostatic closed loop control, a potential equivalent to -850 mV vs. CSE was maintained between REF 1 and the pipe. When evaluating the new closed control method based on measurements of the electrode array, the data collected by the WBE data acquisition unit 1 was fed to a controller program that constantly recalculated the CP current to apply.

For these tests, no cover aiming to simulate a disbonded coating was placed over the electrode array. The current flowing between the auxiliary electrodes was varied in 90 min steps of 1mA from -5 mA to 10 mA.

Before the experimental setup was constructed, the basic geometry and expected current distribution of the electrochemical cell were studied using a finite elements model. The governing equation for the model is the two-dimensional form of Ohm's law. The model was limited to 2D because experimental conditions were maintained constant across the height of the electrochemical cell. The boundary conditions selected for the anode, the electrodes simulating the pipe and the auxiliary electrodes used to inject the stray current into the system, were constant. The current flowing between the auxiliary electrodes was 25 mA. The electrodes simulating the pipe were at a potential of -1.5 V and the anode was at a potential of 2 V. The media conductivity was 0.01 S/m. In addition, when the Ti outer electrodes were part of the model, they were constrained at a potential of 0 V.

Figure 4 presents the potential distribution results for an infinite media. Here the geometry of the experimental arrangement box is included only for reference and does not contribute to the model. As expected, the potentials around the anode and the auxiliary electrode acting as the source of stray current show positive values, while the electrodes simulating the pipe and the auxiliary electrode acting as a sink for the stray current present negative values. More importantly, a gradient is produced over the elongated part of the box where potentials remain nearly constant at cero at the far end, indicating that this would be a suitable location for a remote reference electrode.

Figure 5. presents the simulated potential distribution for a scenario where the conductive media is limited to only the inside of the box and no outer Ti electrodes are used. The boundary conditions for the box walls constrain the current flow to cero. In this case, the potentials along the elongated part of the box remain constant at a value similar to that present near the auxiliary electrode acting as a sink for the stray current. In other words, the elongated part of the box is acting as a Luggin capillary. Consequently, the far end of the elongated part of the box would not be a suitable location for a remote reference electrode in this case because the potential of the electrolyte at this location depends on the magnitude of the stray currents injected to the system.

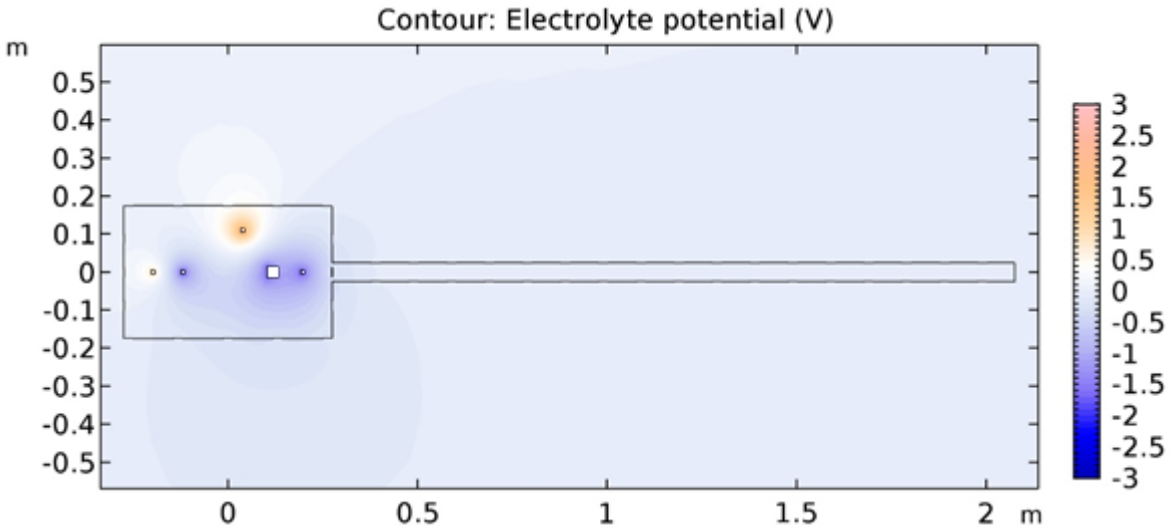

Figure 4. Finite element simulation potential distribution results in an infinite media.

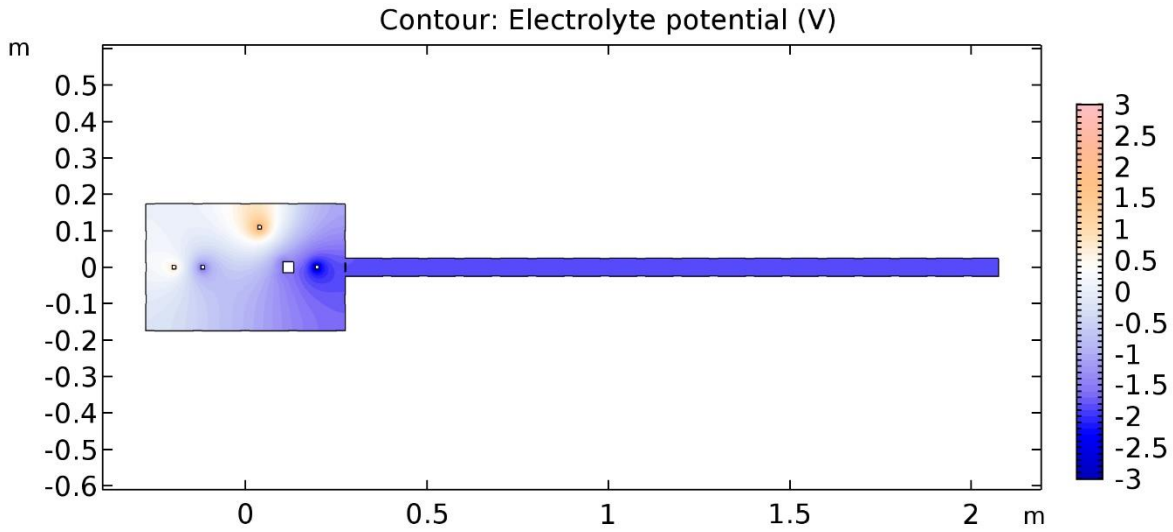

Figure 5. Finite element simulation potential distribution results in an isolated box.

Figure 6 presents the potential distribution results for the finite element simulation for the case where the media is limited to the inside of the box and the Ti outer electrodes are electrically connected among them. In this condition, the potential distribution inside the box is similar to that found for an infinite media and a potential gradient is also produced along the elongated part of the box. Thus, as a conclusion of the simulations, it is expected that the use of outer electrodes would produce a region at the far end of the elongated part of the box where potential is nearly constant and independent of the stray current applied.

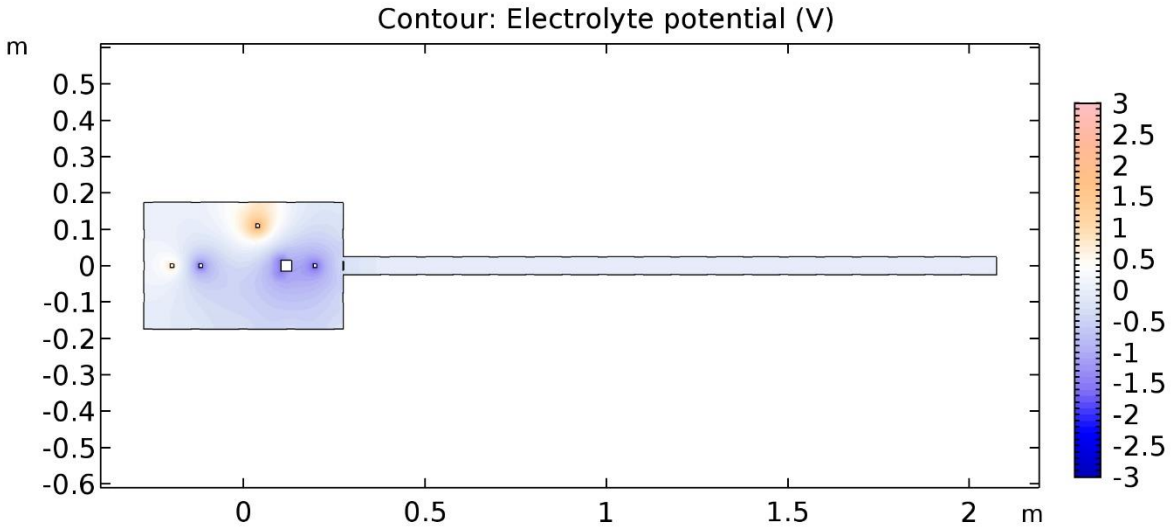

Figure 6. Finite element simulation potential distribution results in a box, using outer electrodes.

3. RESULTS AND DISCUSSION

3.1. Initial proof of concept: Static initial conditions

Figure 7 presents, as an example, the changes in current settings and potential evolution after a random anodic perturbation from the steady state. In this case, the initial anodic perturbation was large and some overshooting is observed before a stable CP current output was achieved. The stable CP current output found produced an IR-drop free potential of about -1.27 V vs. Ag/AgCl (-1.39 V_{CSE}), which is in the overprotection range. This suggests that the current threshold that was arbitrarily selected should be lower for this environment. Figure 8 presents the evolution of the current density maps measured by the electrode array over the same perturbation cycle. Due to the overshooting, it took 15 cycles (300 s) to mitigate most of the anodic activity and overprotection. Then, it took 55 cycles (1100 s) to reach a stable current output with 10 more subsequent cycles of cooling-off period.

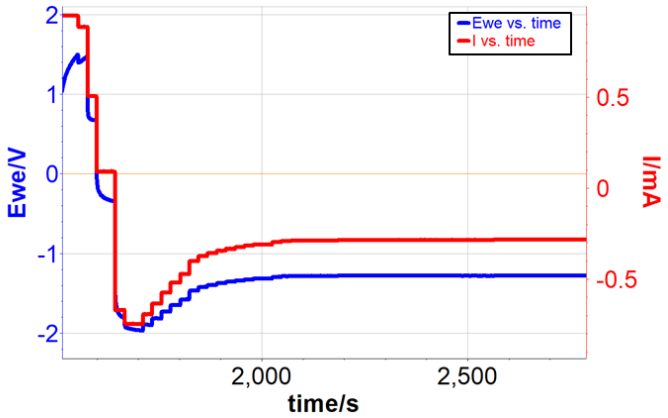

Figure 7. Current settings and potential evolution after typical anodic perturbation with overshooting in 30% WHC sand.

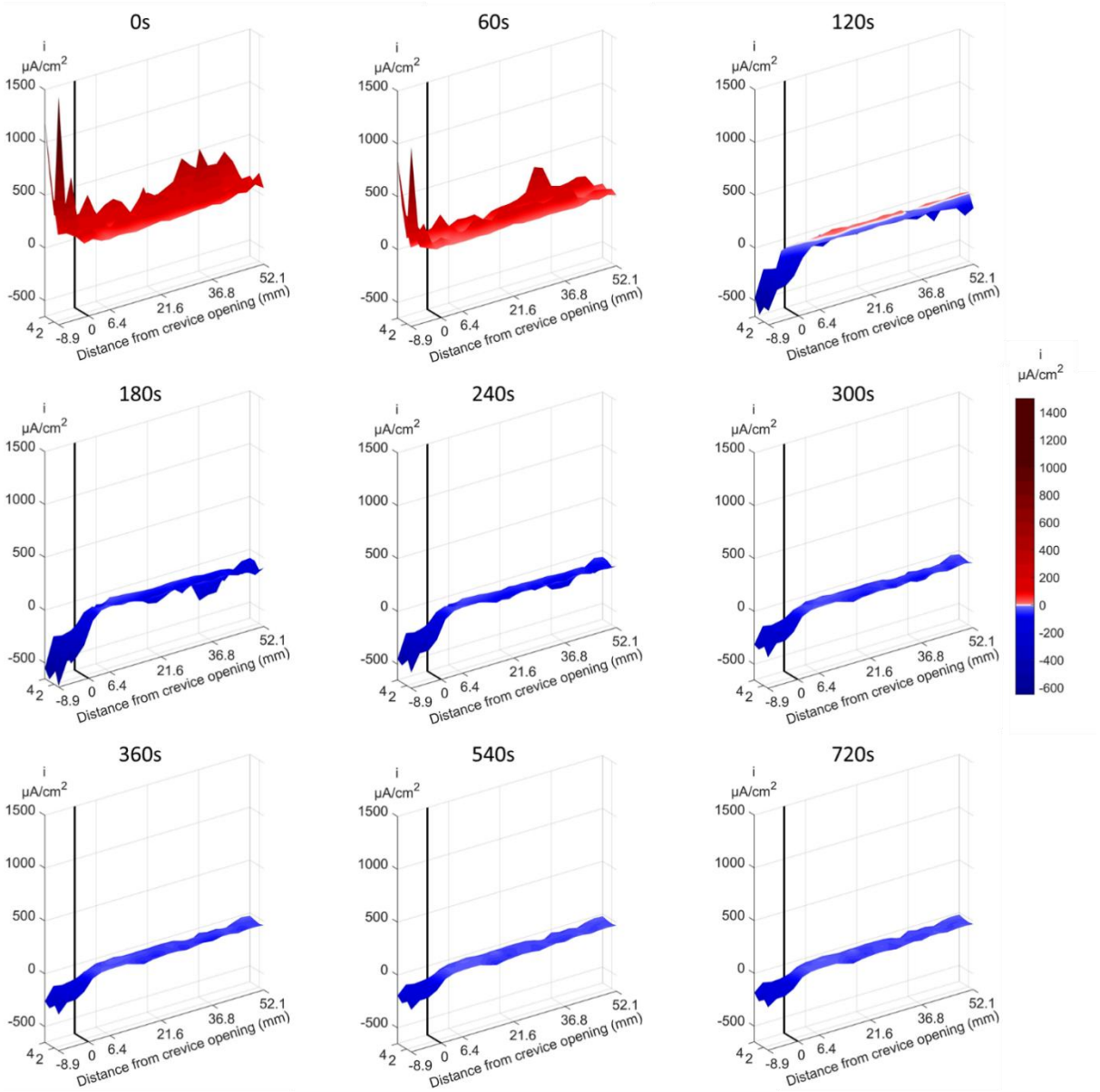

Figure 8. Current density maps evolution after typical anodic perturbation with overshooting in 30% WHC sand.

The effect of Kp on the performance of the controller was evaluated for saturated sand. Being the constant of the proportional controller, Kp is expected to have a dramatic effect on the settling time. This effect can be better appreciated using histograms in Figure 9. For Kp equal to 0.000009, more than 95% of the perturbations were compensated in less than 600 s. Kp factors smaller than 0.000009 resulted in longer settling times due to slower rate of convergence. Kp factors larger than 0.000009 also resulted in longer settling times, but due to increasing levels of overshooting and instability. For Kp equal to 0.000050, the system was unstable. Figure 10 present the unity plot of correction vs. perturbation current for the same conditions. Here it can be appreciated that Kp has an insignificant effect on the accuracy of the method.

Figure 11 presents the unity plot of correction vs. perturbation current for a variety of threshold currents. In general, greater levels of accuracy were found for lower values of threshold current. However, as can be seen in Figure 12, this greater accuracy comes at the expense of longer settling times.

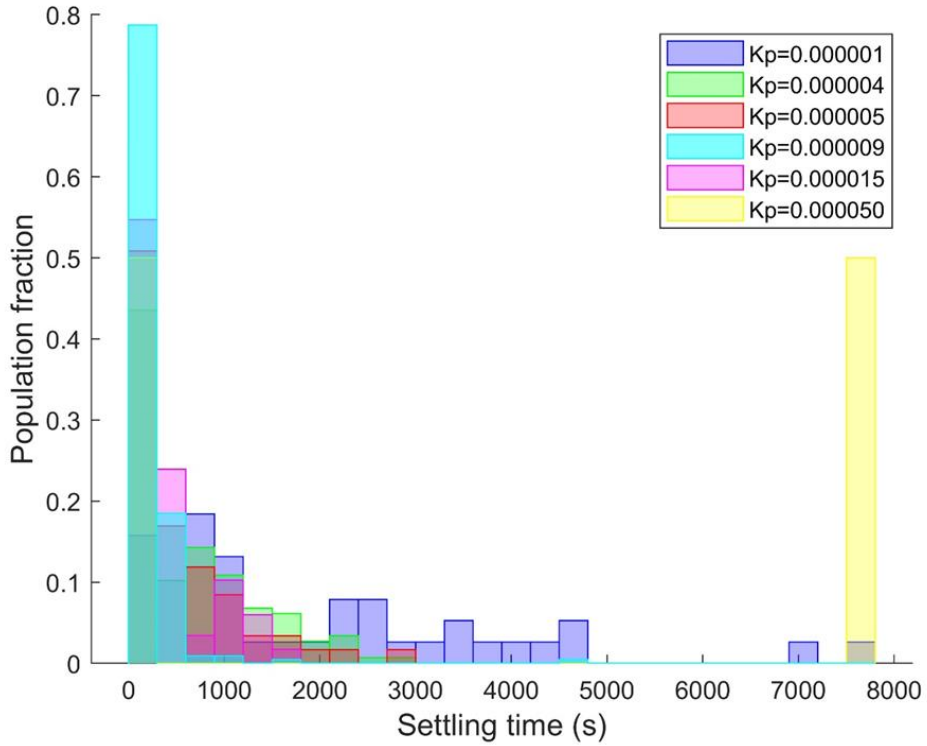

Figure 9. Histograms of settling time in saturated sand for a variety of Kp factors.

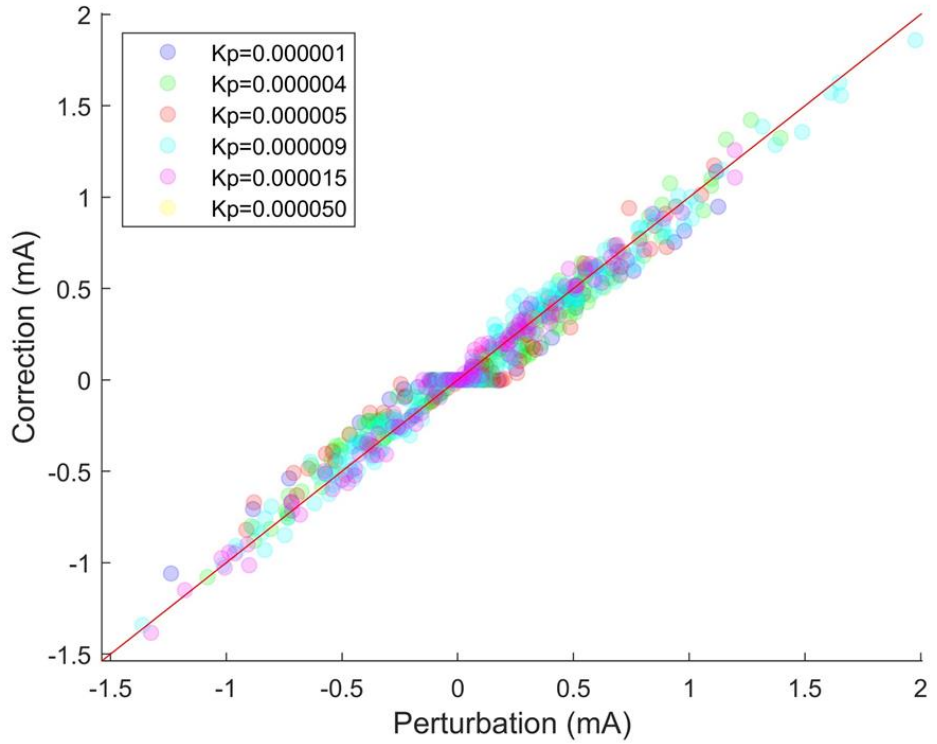

Figure 10. Perturbation vs. correction current unity plot in saturated sand for a variety of Kp factors.

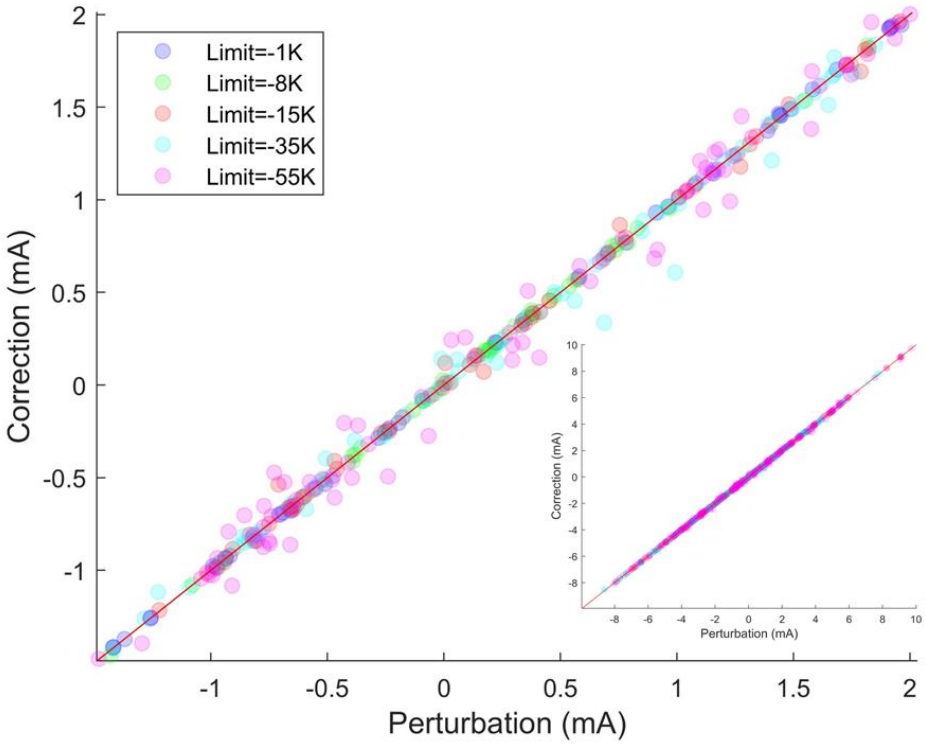

Figure 11. Perturbation vs. correction current unity plot in saturated sand for a variety of threshold currents.

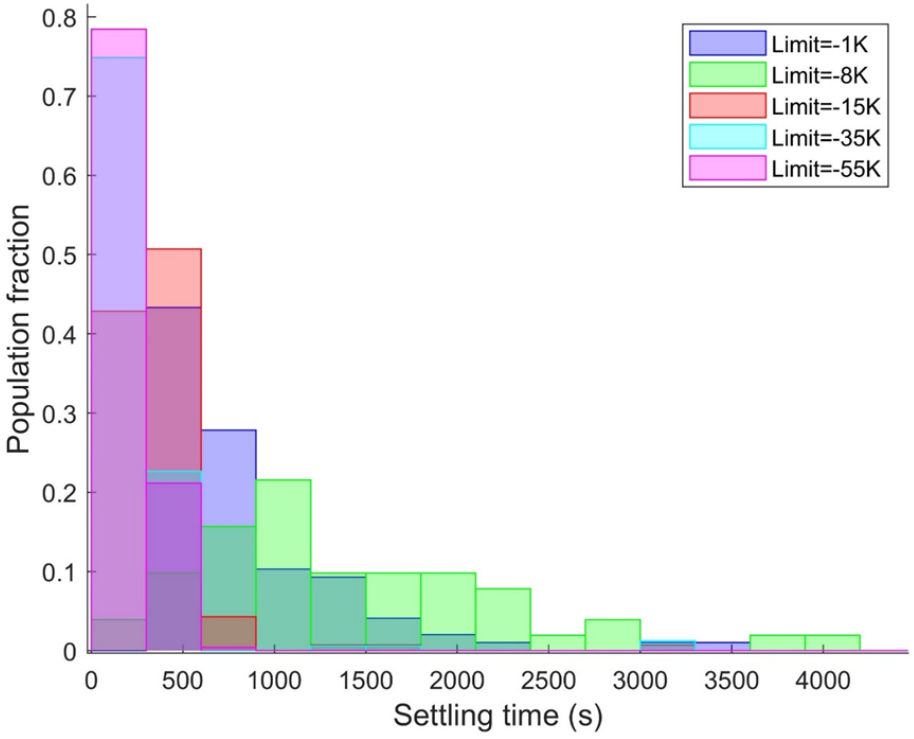

Figure 12. Histograms of settling time in saturated sand for a variety of threshold currents.

3.2. Initial proof of concept: Dynamic conditions

Figures 13 and 14 illustrate the typical results obtained at the two ends of the frequency spectrum. At the low frequency end of the spectrum (Fig. 3), the correction introduced by the controller is almost a mirror image of the test signal. As a result, the CP current output remained almost constant. Figure 4 presents the same type of result as Figure 3, but for the first unstable frequency tested. At this higher frequency the number of data points collected per cycle was only 6, resulting in sharper and noisier curves. The delay produced by the 20 s required for data acquisition, induces a more important phase shift between the signal and correction curves at this frequency. In addition, the correction curve does not show symmetric peaks indicating that the linear controller has difficulty to compensate for the non-linearities of the system at this higher rate of change.

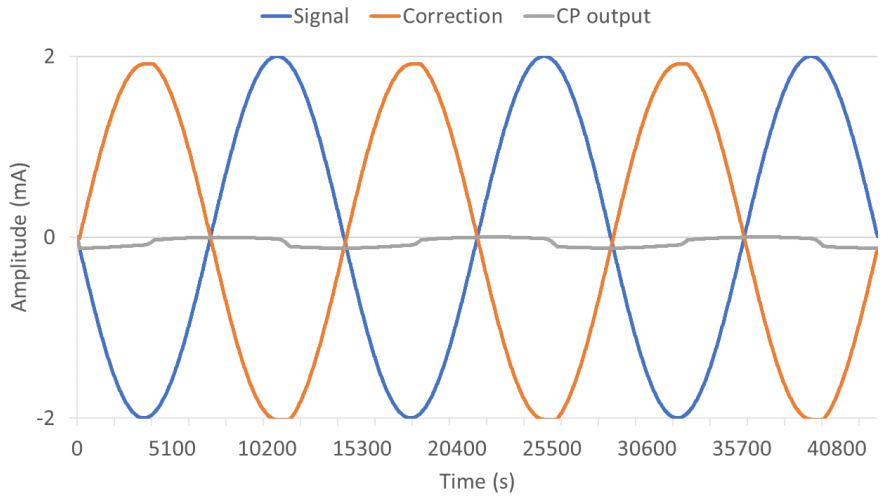

Figure 13. Bandwidth results for saturated sand at 0.07 mHz

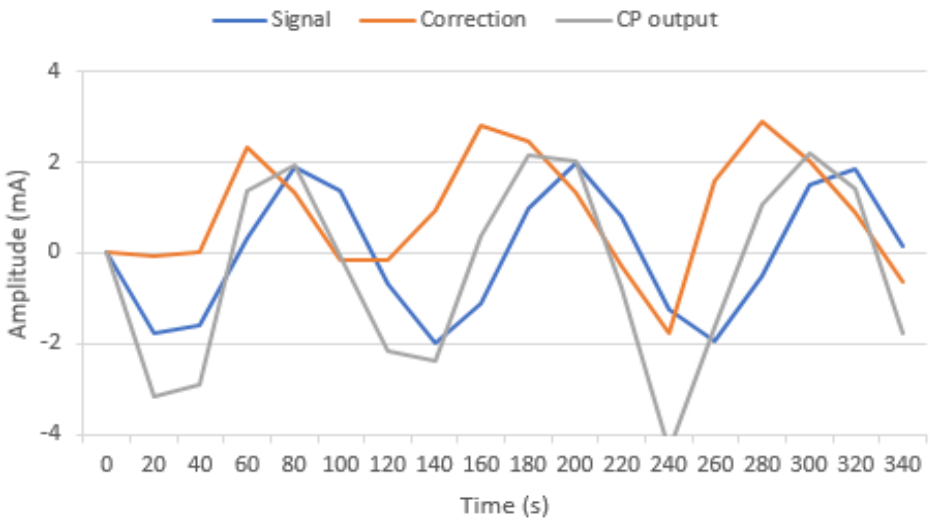

Figure 14. Bandwidth results for saturated sand at 8.78 mHz

Figure 15 presented a Bode plot for the results obtained in saturated sand. From 0.07 mHz to 4.40 mHz the amplitude of the CP output gradually increases as the frequency of the test signal increased, but it maintained under 2 mA. Thus, for frequencies below 4.40 mHz, the closed control loop based on electrode array data partially dumped the test signal. For signals over 4.40 mHz, the delay produced by the slow data acquisition time of the electrode array (20 s) produces an out of phase correction that

results in an CP output signal that is even greater in amplitude than the perturbation signal applied to the system. For these frequencies the use of the close control loop is counterproductive.

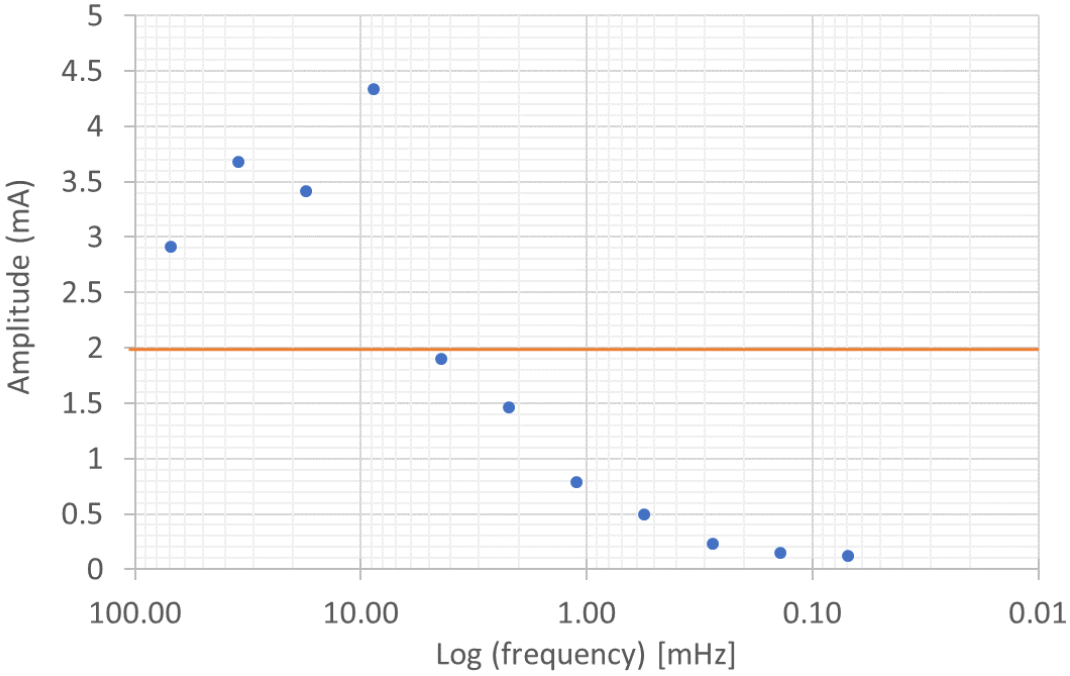

Figure 15. Bode plot for saturated sand

3.3. Back-to-back testing

Figure 16 presents the difference between REF 1 and REF 2 (according to the labels in Fig. 3) for the whole range of stray currents applied. The difference never exceeded 20mV, which is considered the typical variation among reference electrodes of the same type. Figure 17 presents the current flowing through the Ti outer electrodes for all applied stray current values while the controller was in autopotential mode. This information further proves the validity of the remote reference electrode presenting a gradient from electrode 8 onwards which rapidly falls to near zero currents.

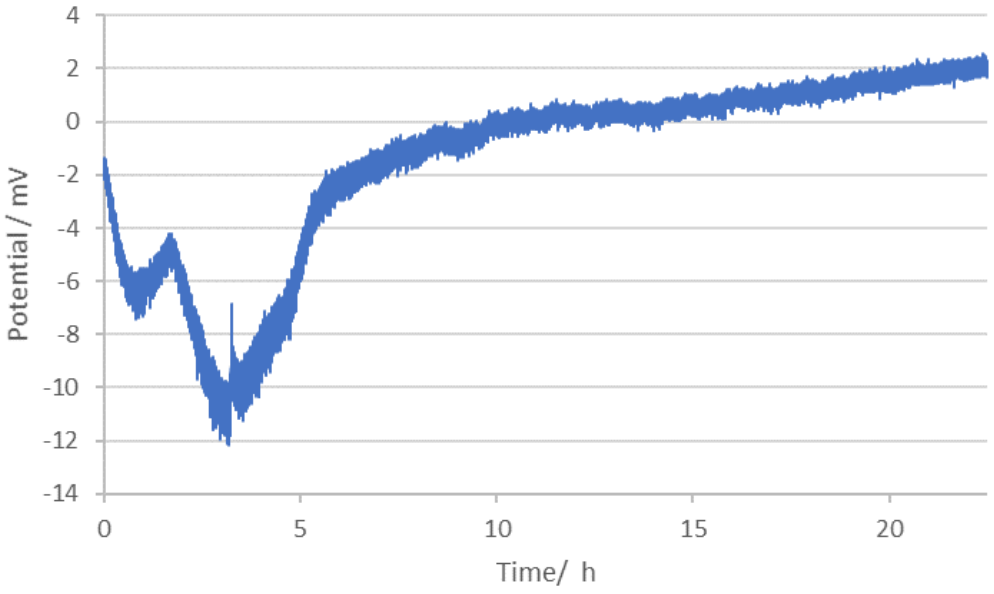

Figure 16. Difference between REF 1 and REF 2 for the whole range of stray currents applied.

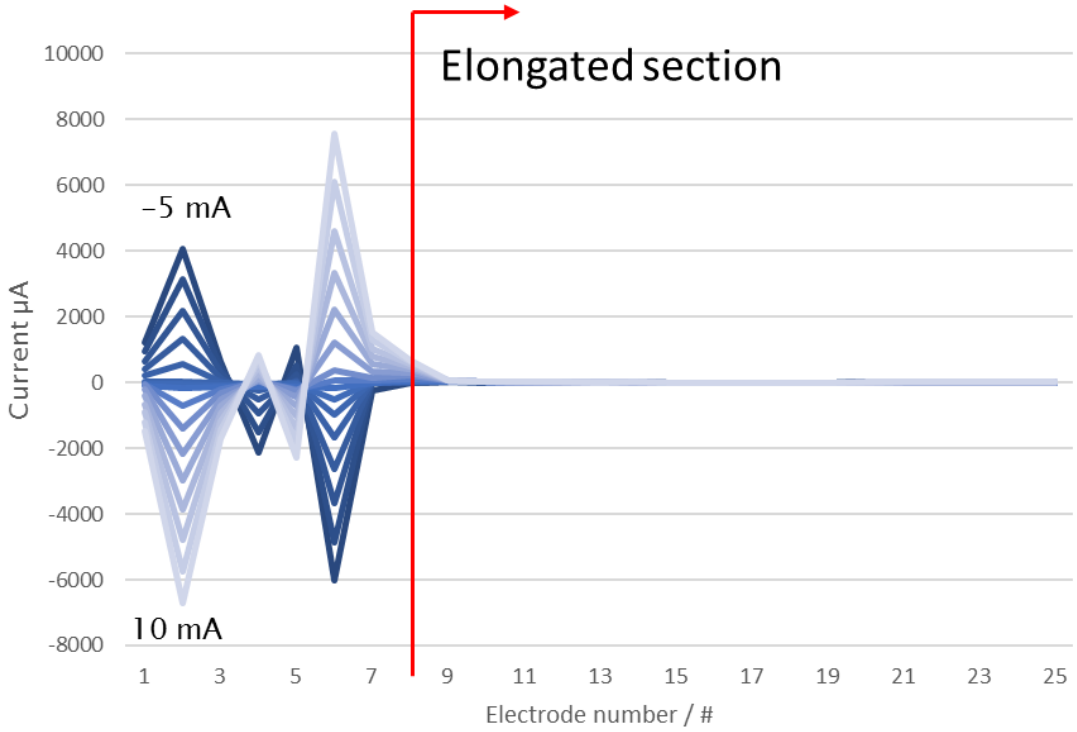

Figure 17. Current registered at the Ti outer electrodes for applied stray currents.

Figures 18 and 19 present the main results of the comparative test performed in sand and 0.01M Na_2SO_4 solution at 60% WHC. In this environment, the autopotential control produced different current density maps when different levels of stray current were applied. Current density maps presented larger cathodic currents when cathodic stay currents were applied and anodic current densities when anodic stray current densities were applied. In contrast, when the new closed control loop was used, no obvious changes in the current density maps are observed despite the effect of changing stray currents. Potentials against the remote reference electrode ranged from -580 mV_{CSE} to -1510 mV_{CSE} when using the new control loop to compensate for the stray currents.

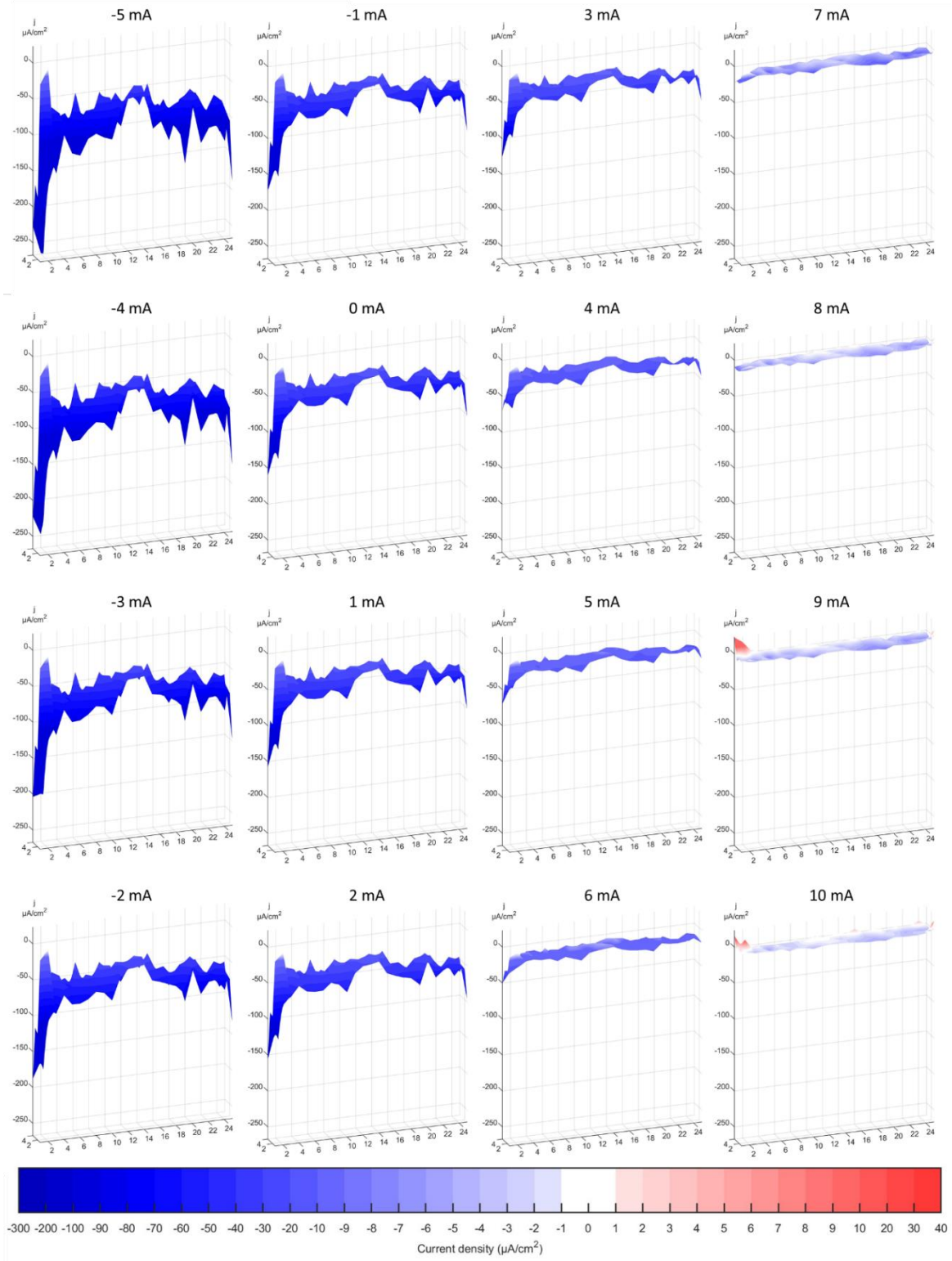

Figure 18. Current density maps obtained under several stray current levels in sand and 0.01M Na_2SO_4 solution at 60% WHC using conventional autopotential control.

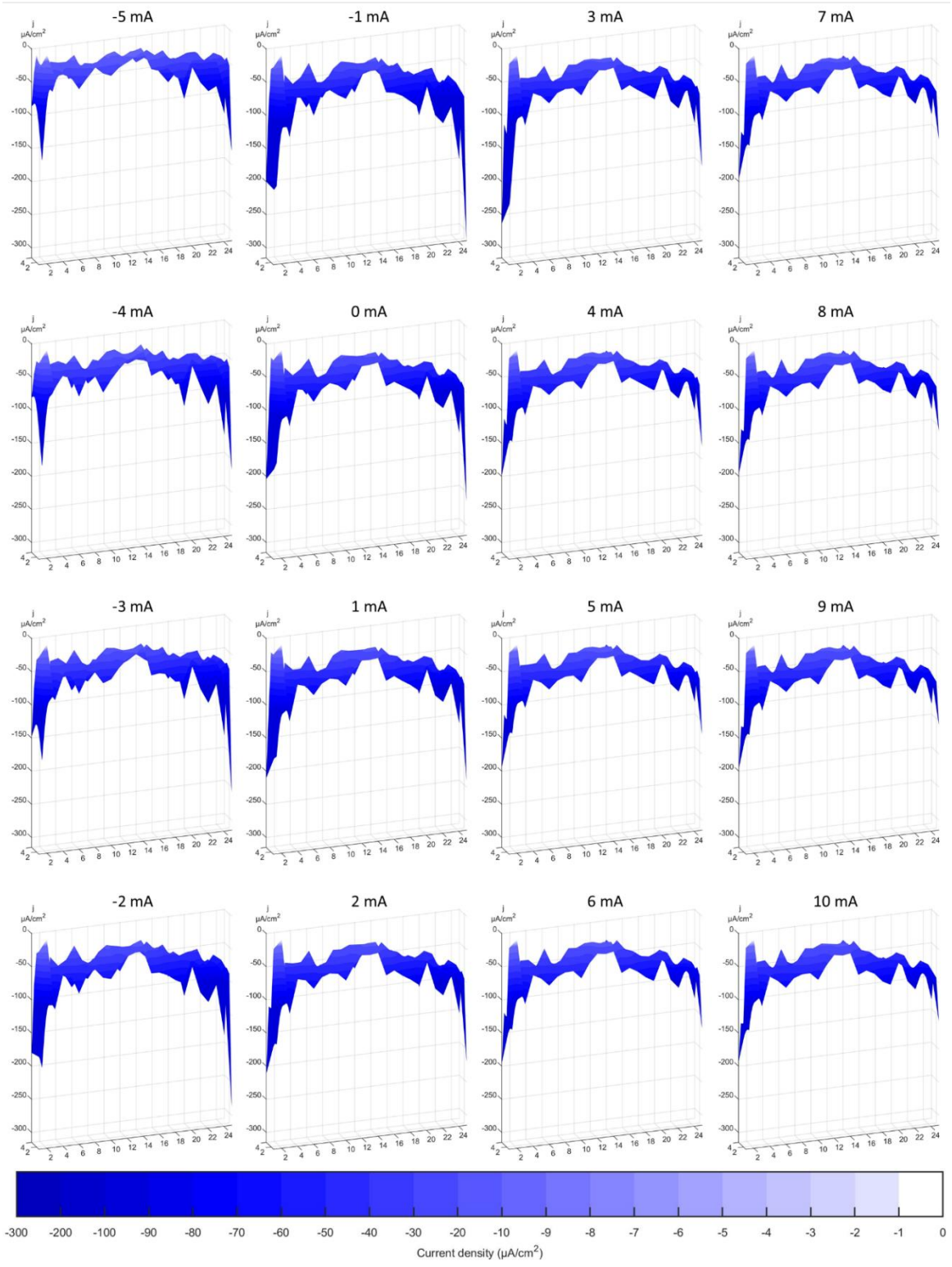

Figure 19. Current density maps obtained under several stray current levels in sand and 0.01M Na_2SO_4 solution at 60% WHC using the new closed control loop based on electrode arrays.

4. CONCLUSIONS

An experimental prototype was built to evaluate the performance of the control algorithm in stable conditions using random perturbations of current. The settling time, accuracy and stability of the system were tested using fixed parameters for the controller. The results were satisfactory, presenting a stable converging behavior for over 2000 different perturbations. The effect of controller parameters on the performance of the system was also evaluated for saturated sand.

The response of the controller to compensate for dynamic changes of increasing frequency has been evaluated. Results indicate that the current limiting factor for the controller bandwidth is the data acquisition rate of the electrode array unit. For practical use, it was concluded that data acquisition rates should be 15 times or higher than the maximum expected frequency of the perturbation. Data acquisition rates fast enough to compensate even for AC stray current should be achievable using off-the-shelve CMOS analog switches.

Finally, a back-to-back evaluation of the closed control loop for CP based on electrode arrays vs. conventional autopotential control was performed. Both closed control methods were evaluated in a stray current scenario where the reference electrode for the autopotential controller was placed at a remote location. Results indicated the limitations of autopotential control, where CP was ineffective at some of the stray current scenarios and overprotection was produced in others. In contrast, the control loop based on electrode arrays presented levels of protection that remained virtually unchanged despite changes in stray current magnitude and polarity.

The work developed through the project moved the closed control loop based on electrode arrays from an incomplete idea into a proven concept. The project findings support the viability of the concept and illustrate its advantages in terms of practicality and performance over current autopotential closed control loops.

5. ACKNOWLEDGEMENTS

This work was funded by the Future Fuels CRC, supported through the Australian Government's Cooperative Research Centres Program. The funding and in-kind support from the APGA RSC is gratefully acknowledged.

6. REFERENCES

1. Cumberland E. Demonstration of the cumberland electrolytic process for preventing corrosion of all metals immersed in liquids. Transactions of the Faraday Society. 1916;11(0):277-81.
2. Kuhn R. Galvanic Currents on Cast Iron Pipe. In: Standards NBo, editor. First Corrosion Conference; December 1928; Washington, Columbia1928.
3. Kuhn RJ. Cathodic protection of underground pipelines from soil corrosion. API Proceedings. 1933;14:153-7.
4. VEC resource manual. In: Victoria ES, editor.: Energy Safe Victoria; 2014. p. 1-110.
5. Neeley GS, inventorMethod of and means for preventing scaling, corrosion, or like action in metallic bodies. United States1932.
6. Spencer PH, inventorCorrosion preventative. United States1936.
7. Miles JA, inventor; John A Miles, assignee. Cathodic protection regulator. United States1956.
8. Jr KDS, inventor; Nokia Bell Labs, assignee. Summing amplifier. United States1941.
9. Vosteen RE, inventorTransistor operational amplifier. United States1963.
10. Hickling A. Studies in electrode polarisation. Part IV-the automatic control of the potential of a working electrode. Transactions of the Faraday Society. 1942;38(0):27-33.
11. Sciences NAo. Biographical Memoirs: Volume 70 (1996). Washington, DC: The National Academies Press; 1996. 1-488 p.
12. Sands ML, inventor; Matthew L Sands, assignee. Electroplating control system. United States1952.

13. Gleason J, inventor; Lockheed Corporation, assignee. Control for impressed current cathodic protection systems. United States1974.
14. Byrne PB, inventor; BASF Catalysts LLC; Engelhard Industries Inc, assignee. Cathodic protection system. United States1966.
15. Dumitrescu V, Ciulin D, Constantin P, inventors; Engelhard Industries Inc, assignee. Cathodic protection system. United States1971.
16. Tietze TN, inventor; Panhandle Eastern Pipe Line Co, assignee. E-Log I field computer. United States1985.
17. NACE. Control of External Corrosion on Underground or Submerged Metallic Piping Systems. Houston, TX, USA: NACE International; 2013. p. 1-60.
18. ISO. Petroleum and natural gas industries - Cathodic protection of pipeline transportation systems. On-land pipelines. Geneva, Switzerland: ISO; 2003. p. 1-40.
19. AS. Cathodic protection of metals. Pipes and Cables. Sydney, Australia: Australia Standards; 2004. p. 1-76.
20. Jr FHS, inventor; BASF Catalysts LLC, Engelhard Minerals and Chemicals Corp, assignee. Sampling and control system for cathodic protection. United States1972.
21. Ferry CR, Peterson MF, inventors; Harco Corp, assignee. Cathodic protection method and apparatus. United States1978.
22. Merrick LH, inventor; Harco Corp, assignee. Method and apparatus for determining the reference voltage in an impressed current corrosion protection system. United States1979.
23. Birchmeier JR, Ruck GT, Thompson NG, Barlo TJ, inventorsMethod and apparatus for measuring the polarized potential of a buried or submerged structure protected by impressed current. United States1986.
24. Walcott KJ, Thompson NG, Ruck GT, Helton SB, inventors; Gas Technology Institute, assignee. Measurement of the polarized potential of buried pipeline having impressed current cathodic protection. United States1989.
25. Thompson NG, Lawson KM, inventors; CC Technologies Systems Inc, assignee. Coupon test station for monitoring the effectiveness of cathodic protection. United States1998.
26. Caudill DL, Thompson NG, Lawson KM, inventors; CC Technologies Systems Inc, assignee. Coupon monitor for cathodic protection system. United States2000.
27. Stern M, Roth RM. Anodic behavior of iron in acid solutions. J Electrochem Soc. 1957;104(6):390-2.
28. Barbalat M, Lanarde L, Caron D, Meyer M, Vittonato J, Castillon F, et al. Electrochemical study of the corrosion rate of carbon steel in soil: Evolution with time and determination of residual corrosion rates under cathodic protection. Corros Sci. 2012;55(0):246-53.
29. Barbalat M, Caron D, Lanarde L, Meyer M, Fontaine S, Castillon F, et al. Estimation of residual corrosion rates of steel under cathodic protection in soils via voltammetry. Corros Sci. 2013;73(0):222-9.
30. Mckubre MCH, Syrett BC, inventors; Electric Power Research Institute, assignee. In situ monitoring of corrosion rates of polarized or unpolarized metals. Europe1988.
31. Syrett BC, McKubre MCH, inventors; Electric Power Research Institute, assignee. Device for in-situ monitoring of corrosion rate of cathodically polarized metals. United States1987.
32. McKubre MCH, Syrett BC, inventors; Electric Power Research Institute, assignee. Device for in situ monitoring of corrosion rates of polarized or unpolarized metals. United States1991.
33. Bosch R-W, Bogaerts WF, inventors; Katholieke Universiteit Leuven, assignee. Apparatus and method for electrochemical corrosion monitoring. United States2001.
34. Tan Y-J, inventorMethod and apparatus for measuring localized corrosion and other heterogeneous electrochemical processes. United States2000.
35. Varela F, Tan YJ, Forsyth M. A Novel Approach for Monitoring Pipeline Corrosion under Disbonded Coatings. 10th International Pipeline Conference; September 2014; Calgary, Canada2014. p. 1.
36. Varela F, Tan YJ, Forsyth M. Monitoring Cathodic Shielding and Corrosion under Disbonded Coatings 19th International Corrosion Congress; Novermber 2014; Jeju, Korea2014. p. 1.

37. Varela F, Tan MYJ, Forsyth M. An electrochemical method for measuring localized corrosion under cathodic protection. ECS Electrochem Lett. 2015;4(1):C1-C4.
38. Varela F, Tan MYJ, Forsyth M. Understanding the effectiveness of cathodic protection under disbonded coatings. Electrochim Acta. 2015;186:377-90.
39. Varela F, Tan MY, Forsyth M. Electrochemical Method for Studying Localized Corrosion beneath Disbonded Coatings under Cathodic Protection. J Electrochem Soc. 2015;162(10):C515-C27.
40. Varela F. Electrochemical methods for monitoring localized corrosion under cathodic protection [Thesis y publication]. Waurn Ponds, Victoria, Australia: Deakin University; 2015.